Journal of Physics: Conference Series

PAPER • **OPEN ACCESS**

Active vibration control of planetary gears by pole placement

To cite this article: K A Olanipekun *et al* 2019 *J. Phys.: Conf. Ser.* **1264** 012004

IOP Conf. Series: Journal of Physics: Conf. Series **1264** (2019) 012004 doi:10.1088/1742-6596/1264/1/012004

Active vibration control of planetary gears by pole placement

K A Olanipekun, E Rustighi and N S Ferguson

Institute of Sound and Vibration Research, University of Southampton, SO17 1BJ, UK

Abstract. This numerical study focuses on the assignment of poles to a planetary gear train to avoid resonance, which can cause the failure of the system. The control strategy is output feedback, which involves feeding back the displacement and velocity to achieve active stiffness and damping respectively. The reverse process was considered. This occurs when the predicted control gains were assigned by the actuators, which were placed on the translational directions of either the carrier or the sun gear bearing mounted on the shaft. In addition, the closed-loop poles were assigned in the case whereby the actuators were positioned in the translational directions of either the carrier or the sun gear. The active control was considered using both the fixed and rotating frames of reference at a carrier speed of 100 rpm. Numerical examples are presented using both reference frames with the sensors and actuators collocated. The results show that the poles of the modes with lower frequencies, which are predominantly translational modes, can be shifted while the poles of the higher modes, which are predominantly rotational remain unchanged.

1. Introduction

Planetary gears are widely used in many applications such as power transmission in automotive vehicles, aircraft, turbines, power screw, etc. A planetary gear train typically comprises a carrier, ring, sun and multiple planet gears. It has a better load carrying capacity than the parallel shaft gear, because of the planet gears in the train. The number of planetary gears required is determined by the load to be carried by the system. Another comparative advantage over parallel shaft gears is that the coaxial arrangement of the shafts lead to a compact layout (Figure 1 (a) and (b)). Also, different gear ratios can be obtained by typically keeping one of the central members (i.e. either the carrier, ring or sun gear) stationary. These configurations make them versatile in their application.

However, with the advantages of planetary gears over the parallel shaft gears discussed, there can still be vibration and noise during operation. Some of the causes of vibration and noise are the time variation in the mesh stiffness, profile error in the gear teeth, misalignment of shafts, etc. In helicopter cabins, planetary gears are the main noise source where the sound level measured can be more than 100 dB [1]. To prevent the structural failure associated with vibration of planetary gears, effort must be made to control the vibration [2].

There are some methods of vibration control that have been utilized to mitigate gear vibration. A passive method involves changing the physical properties of the system, like mesh phasing or tip relief on the teeth which have been implemented by some researchers. Seager [3] shows that some difficult harmonic component can be neutralized by suitably choosing the number of teeth. He concluded that the conditions to neutralize the mesh frequency components acting on the central members are if the ratio of the number of teeth of the sun gear to the number on the planet gear is not equal to an integer. Secondly, the source is reduced if the number of teeth on the planet gear plus or minus one divided by the number of planet gears is not an integer. The effectiveness of phasing the planet gear to reduce vibration of planetary gear was studied by Parker [4]. Planet phasing involves configuration of the planet gears, as well as choosing the number of teeth such that self-equilibration of the mesh forces lead to reduction in the net forces and torques acting on the carrier, ring and sun gears. Phasing reduces the

vibration due to some harmonics of the mesh frequency. Richards and Pines [5], presented a passive method to mitigate transmitted vibration generated by gear mesh. A periodic shaft comprising identical elements connected together was designed so as to create stop and pass band regions in the frequency spectra. Transmitted vibrations from the gear mesh to the bearing support were mitigated at various operating speeds. Tharmakulasingam et al. [6] simulated how the transmission error will be affected by modifying the tooth profile. The result of this showed that there is a significant reduction in the transmission error in the spur gear with tooth profile modification (tip relief) compared to the spur gear without tooth profile modification.

However, active vibration control method is more flexible than passive method because the control force can be adjusted based on the vibration characteristics during operation. In addition, passive methods have limitations when several modes are excited. Montague et al. [7] presented a means of reducing mesh vibration in a parallel axis gear by feedforward control using piezoelectric actuators. They presented the principle of the method by an analysis of a vibrating linear system being excited by a harmonic force. The result shows a 70% reduction in the gear mesh vibration at 4500 Hz. Active vibration control method was used by Rebbechi et al. [8] to reduce gear mesh vibration using magnetostrictive actuators inside the gearbox. A feedforward controller was used to determine the required amplitude and phase of the control force applied to the shaft to reduce vibration at the feet of gearbox housing. The vibration was reduced at the first three harmonics of the gear mesh frequency.

This paper presents the theory for pole placement applied to a planetary gear. This theory is an extension of that developed by Mottershead et al. [9] and the model is an extended model developed by Parker [10]. The method is based on output feedback, where the sensor and actuator can be collocated. In practice, there is no need to determine the global mass, damping and stiffness matrices as the measured receptance from the open loop system is used. The aim of the pole placement is to shift the natural frequencies of the planetary gear in order to avoid resonance through displacement feedback. Active damping will also be added through velocity feedback. Numerical examples will be demonstrated, first using a fixed frame of reference to determine the gains after pole assignment. These gains will be assigned to the system using a rotating frame of reference to determine the equivalent poles. These equivalent poles will subsequently be assigned to the system using a fixed frame of reference and the resulting feedback gains will be used to calculate the control force required using fixed frame of reference. Subsequently, the equivalent control force determined will be applied using the fixed frame of reference.

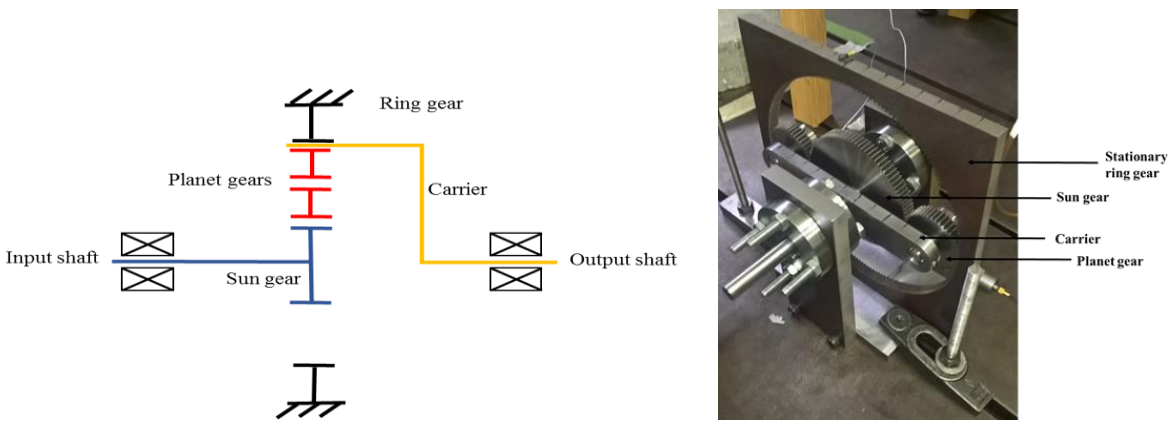

(a) (b)

Figure 1. (a) Schematic diagram of planetary gear showing the input and the output (b) Experimentally based planetary gear.

2. Theoretical analysis using a fixed frame of reference

The second order general dynamic equation of motion for the planetary gear system using a fixed frame of reference in the Laplace domain is written as:

$$[\mathbf{s}^2\mathbf{M} + \mathbf{s}\mathbf{C}_b + (\mathbf{K}_b + \mathbf{K}_m)]\mathbf{q}(\mathbf{s}) = \mathbf{F}_{te}(\mathbf{s}) + \mathbf{B}\mathbf{U}(\mathbf{s}) \qquad (1)$$

$$\mathbf{F}_{te} = k_{sn}e_{sn}\begin{bmatrix}0 & 0 & 0 & 0 & 0 & 0 & \sin\psi_{sn} & \cos\psi_{sn} & 1 & -\sin\alpha_s & -\cos\alpha_s & -1 & 0 & 0 & 0\end{bmatrix}^T$$

$$\psi_{sn} = \psi_n - \alpha_s$$

where, $\mathbf{M}, \mathbf{C}_b, \mathbf{K}_b, \mathbf{K}_m \in \Re^{n\times n}$; $\mathbf{M} = \mathbf{M}^T, \mathbf{C}_b = \mathbf{C}_b^T, \mathbf{K}_b = \mathbf{K}_b^T, \mathbf{K}_m = \mathbf{K}_m^T$ are the mass, damping, bearing and mesh stiffnesses respectively. The notation $\mathbf{B} \in \Re^{m\times n}$ is the control force distribution matrix $\mathbf{U}(\mathbf{s}) \in \Re^{m\times 1}$ and is the control force, while $\mathbf{F}_{te} \in \Re^{m\times 1}$ is the disturbance due to the transmission error in the sun-planet mesh. The pressure angle and planet positions are denoted by α_s and ψ_n (Figure 3).

The feedback control law can be expressed as:

$$\mathbf{U}(\mathrm{s}) = -(\mathbf{G} + \mathrm{s}\mathbf{F})\mathbf{q}_{op}(\mathrm{s}) \qquad (2)$$

The matrices **G** and **F** give the output and gains, which are directly proportional to active stiffness and damping respectively. The output equation is written as

$$\mathbf{q}_{op}(\mathrm{s}) = \mathbf{D}\mathbf{q}(\mathrm{s}) \qquad (3)$$

For collocated sensors and actuators, $\mathbf{B}^T = \mathbf{D} \in \Re^{m\times n}$, where **D** is the sensor distribution matrix and vector $\mathbf{q}_{op}(\mathrm{s})$ is the output. If **U(s)** is substituted into Equation (1), then

$$\mathbf{q}(\mathbf{s}) = [\mathbf{s}^2\mathbf{M} + \mathbf{s}(\mathbf{C}_b + \mathbf{BFD}) + (\mathbf{K}_b + \mathbf{K}_m + \mathbf{BGD})]^{-1}\mathbf{F}_{te}(\mathbf{s}) \qquad (4)$$

where $[\mathbf{s}^2\mathbf{M} + \mathbf{s}(\mathbf{C}_b + \mathbf{BFD}) + (\mathbf{K}_b + \mathbf{K}_m + \mathbf{BGD})]^{-1}$ is the closed loop displacement per mesh excitation matrix in the fixed frame of reference. The term $\mathbf{s}(\mathbf{C}_b + \mathbf{BFD})$ provides active damping while $(\mathbf{K}_b + \mathbf{K}_m + \mathbf{BGD})$ changes the natural frequencies of the system. The open loop receptance matrix is given by

$$\mathbf{H}(\mathbf{s}) = [\mathrm{s}^2\mathbf{M} + \mathrm{s}\mathbf{C}_b + (\mathbf{K}_b + \mathbf{K}_m)]^{-1} \qquad (5)$$

If Equation (4) is pre-multiplied both sides by the **H(s)**, one obtains,

$$\mathbf{q}(\mathrm{s}) = \frac{\mathrm{adj}[\mathbf{I}+\mathbf{H}(\mathbf{s})\mathbf{B}(\mathbf{G}+\mathrm{s}\mathbf{F})\mathbf{D}]}{\det[\mathbf{I}+\mathbf{H}(\mathbf{s})\mathbf{B}(\mathbf{G}+\mathrm{s}\mathbf{F})\mathbf{D}]}\mathbf{H}(\mathrm{s})\mathbf{F}_{te}(\mathrm{s}) \qquad (6)$$

The eigenvalues μ_j that make the denominator equal to zero are known as the poles. The eigenvalues λ_i that make the numerator of Equation (6) equal to zero are known as zeros. Only pole assignment will be considered in this paper. The schematic diagram of the control system is shown in Figure 2, where the disturbance is applied at the input and the output is fed back to achieve stability in the system.

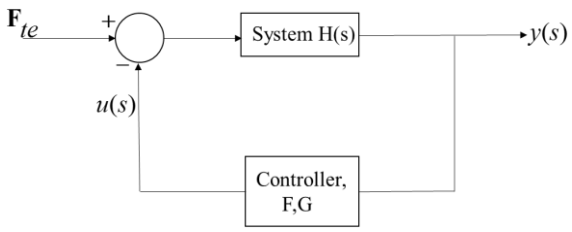

Figure 2. Schematic diagram of closed loop feedback control system.

3. Theoretical analysis using a rotating frame of reference

The control algorithm in the rotating frame of reference can be similarly obtained. The **M**, **C** and **K** matrices are different as well as the coordinate system. This can be analyzed using Figure 3, where the dynamics of the rigid bodies were modelled using a rotating frame of reference fixed to the carrier. The coordinate basis (*i*, *j*, *k*) in Figure 2 rotates with constant angular speed of the carrier Ω_c .

The second order dynamic equation of motion for the planetary gear system using a rotating frame of reference in the Laplace domain is

$$[s^2\bar{\mathbf{M}} + s(\Omega_c \mathbf{G}_y + \bar{\mathbf{C}}_b) + (\bar{\mathbf{K}}_b + \bar{\mathbf{K}}_m + \Omega_s \mathbf{K}_d - \Omega_c^2 \mathbf{K}_\Omega)]\bar{\mathbf{q}}(\mathbf{s}) = \mathbf{w}(\mathbf{s}) + \bar{\mathbf{B}}\bar{\mathbf{U}}(\mathbf{s}) \tag{7}$$

where $\bar{\mathbf{M}}, \bar{\mathbf{C}}_b, \bar{\mathbf{K}}_b, \bar{\mathbf{K}}_m, \mathbf{G}_y \in \Re^{n\times n}$ are the mass, damping, bearing stiffness, mesh stiffness and Coriolis matrix respectively. $\bar{\mathbf{M}} = \bar{\mathbf{M}}^T, \mathbf{K}_b = \bar{\mathbf{K}}_b^T, \bar{\mathbf{K}}_m = \bar{\mathbf{K}}_m^T, \bar{\mathbf{K}}_\Omega = \bar{\mathbf{K}}_\Omega^T, \bar{\mathbf{C}}_b = \bar{\mathbf{C}}_b^T$ while the $\mathbf{G_y}$ and $\mathbf{K_d}$ matrices are skew-symmetric. $\bar{\mathbf{B}} \in \Re^{m\times n}$ is the control force distribution matrix and $\bar{\mathbf{U}}(\mathbf{s}) \in \Re^{m\times 1}$ is the control force, while $\mathbf{w} \in \Re^{m\times 1}$ is the disturbance due to the transmission error.

The output equation is written as:

$$\bar{\mathbf{q}}_{op}(\mathrm{s}) = \bar{\mathbf{D}}\bar{\mathbf{q}}(\mathrm{s}) \tag{8}$$

From Equation (2), the control force using a rotating frame of reference can be derived using the transformation matrix, **T**:

$$\mathbf{T} = \begin{bmatrix} \cos\Omega_c t & -\sin\Omega_c t & 0 \\ \sin\Omega_c t & \cos\Omega_c t & 0 \\ 0 & 0 & 1 \end{bmatrix} \tag{9}$$

Since the control force will not be applied to the rotational degree of freedom, the matrix **T** is reduced to a 2×2 matrix, which implies the third row and column will be ignored. The expression in Equations (10, 11 and 12) shows the control forces applied in the horizontal and vertical directions of either the carrier or the sun gear.

$$\bar{\mathbf{B}}\bar{\mathbf{U}} = -\bar{\mathbf{B}}(\bar{\mathbf{G}} + \Omega_C \bar{\mathbf{F}}\mathbf{J} + \mathrm{s}\bar{\mathbf{F}})\bar{\mathbf{D}}\bar{\mathbf{q}}(\mathrm{s}) \tag{10}$$

where

$$-\Omega_c \begin{bmatrix} 0 & -1 \\ 1 & 0 \end{bmatrix} = \mathbf{T}^T\dot{\mathbf{T}} \tag{11}$$

$$\mathbf{J} = \begin{bmatrix} 0 & -1 \\ 1 & 0 \end{bmatrix} \tag{12}$$

Substituting for $\bar{\mathbf{B}}\bar{\mathbf{U}}$ in Equation (7), one obtains,

$$[s^2\bar{\mathbf{M}} + s(\Omega_c \mathbf{G}_y + \bar{\mathbf{C}}_b + s\bar{\mathbf{B}}\bar{\mathbf{F}}\bar{\mathbf{D}}) + (\bar{\mathbf{K}}_b + \bar{\mathbf{K}}_m + \Omega_s \mathbf{K}_d - \Omega_c^2 \bar{\mathbf{K}}_\Omega + \bar{\mathbf{B}}\bar{\mathbf{G}}\bar{\mathbf{D}} + \Omega_c \bar{\mathbf{B}}\bar{\mathbf{F}}\mathbf{J}\bar{\mathbf{D}})]\bar{\mathbf{q}}(\mathbf{s}) = \bar{w}(\mathbf{s}) \tag{13}$$

The open loop displacement per mesh excitation matrix is in this case is

$$\bar{\mathbf{H}}(\mathbf{s}) = [s^2\bar{\mathbf{M}} + s(\Omega_s \mathbf{G}_y + \bar{\mathbf{C}}_b) + (\bar{\mathbf{K}}_b + \bar{\mathbf{K}}_m + \Omega_s \mathbf{K}_d - \Omega_c^2 \bar{\mathbf{K}}_\Omega)]^{-1} \tag{14}$$

and

$$\bar{\mathbf{q}}(s) = \frac{adj[\mathbf{I}+\bar{\mathbf{H}}(\mathbf{s})\bar{\mathbf{B}}(\bar{\mathbf{G}}+\Omega_c\bar{\mathbf{F}}\mathbf{J}+s\bar{\mathbf{F}})\bar{\mathbf{D}}]}{\det[\mathbf{I}+\bar{\mathbf{H}}(\mathbf{s})\bar{\mathbf{B}}(\bar{\mathbf{G}}+\Omega_c\bar{\mathbf{F}}\mathbf{J}+s\bar{\mathbf{F}})\bar{\mathbf{D}}]}\bar{\mathbf{H}}(s)\bar{\boldsymbol{w}}(s) \tag{15}$$

The corresponding eigenvalues μ_j are equal to poles given as solutions to $\det(\mathbf{I} + \bar{\mathbf{H}}(\mu_j)\bar{\mathbf{B}}(\bar{\mathbf{G}} + \Omega_c\bar{\mathbf{F}}\mathbf{J} + \mu_j\bar{\mathbf{F}})\bar{\mathbf{D}}) = \mathbf{0}$. The corresponding eigenvalues λ_i are equal to zeros given as solutions to $\mathrm{adj}(\mathbf{I} + \bar{\mathbf{H}}(\lambda_i)\bar{\mathbf{B}}(\bar{\mathbf{G}} + \Omega_c\bar{\mathbf{F}}\mathbf{J} + \lambda_i\bar{\mathbf{F}})\mathbf{D})\bar{\mathbf{H}}(\lambda_i) = \mathbf{0}$.

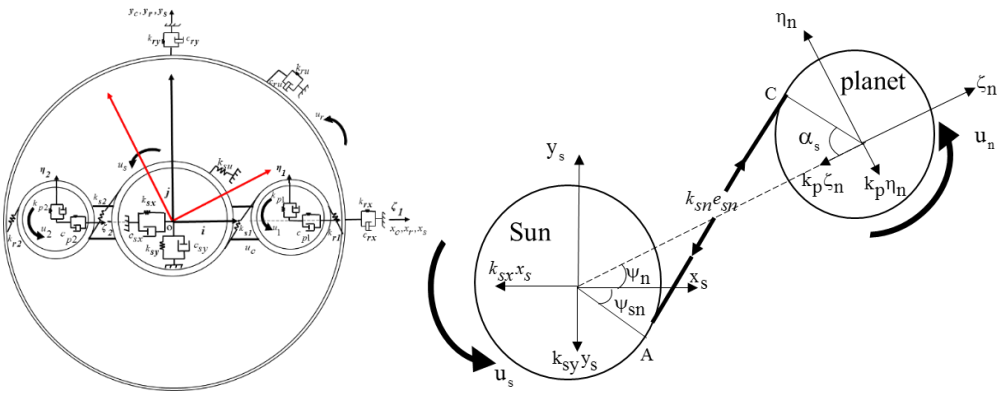

(a) (b)

Figure 3. (a) Lumped parameter model of planetary gears and the coordinates. (b) Sun-planet mesh model showing pressure line AC and the mesh force $k_{sn}e_{sn}$ due to transmission error e_{sn}.

4. Numerical examples of pole assignment to the carrier

The pole placement will firstly be applied to the carrier only, in the vertical and horizontal directions simultaneously using the fixed and rotating frames of reference. One carrier speed will be considered when assigning poles to the carrier using rotating frames of reference.

Table A1. Parameters of the system

	Carrier	**Ring**	**Sun**	**Planet**
Mass (kg)	1.030	4.300	2.212	0.578
I/r^2(kg)	0.1048	1.047	0.9730	0.2502
Base circle diameter (mm		261.00	134.00	63.40
Bearing stiffness (N/m)	0.76×10^6	4.5×10^7	2.0×10^6	14×10^6
Damping coefficient (Ns/m)	16.98	278.21	42.067	56.893
Mesh stiffness k_{sn} (N/m)			3.3×10^8	
Torsional stiffness of the ring K_{ru} (N/m)		1.5×10^9		
Torsional damping of the ring C_{ru} (Ns/m)		1606.24		
Pressure angle $\alpha_r = \alpha_s$		20°		
Transmission error sun-planet mesh e_{sn} (mm)		1.05		

4.1. Pole assignment to the carrier using a fixed frame of reference

Two pairs of complex conjugate poles at $\lambda_{1,2} = -15 \pm 800i$ and $\lambda_{3,4} = -50 \pm 3000i$ were assigned using two actuators supplying feedback control forces to the carrier in the horizontal and vertical directions.. The actuator distribution matrix $\mathbf{B}_c \in \Re^{15\times 2}$ and the sensor distribution matrix $\mathbf{D}_c \in \Re^{2\times 15}$ are then

$$\mathbf{D} = \mathbf{B}^{\mathrm{T}} = \begin{bmatrix} 1 & 0 & 0 & 0 & 0 & 0 & 0 & 0 & 0 & 0 & 0 & 0 & 0 & 0 & 0 \\ 0 & 1 & 0 & 0 & 0 & 0 & 0 & 0 & 0 & 0 & 0 & 0 & 0 & 0 & 0 \end{bmatrix} \tag{16}$$

In this case, $q_{1op} = x_c$ and $q_{2op} = y_c$. The open-loop displacement per mesh excitation are the values of s corresponding to the chosen closed loop poles

$$\mathbf{H}(\lambda_j) = (\mathbf{M}\lambda_j^2 + \mathbf{C}_b\lambda_j + \mathbf{K}_b + \mathbf{K}_m)^{-1}, \qquad j = 1, ..., 4$$

The four characteristic equations, which are nonlinear in control gains, **G** and **F**, can be written as

$$\det(\mathbf{I} + \mathbf{H}(\lambda_j)\mathbf{B}(\mathbf{G} + \lambda_j\mathbf{F})\mathbf{B}^{\mathrm{T}}) = 0, \quad j = 1, ..., 4$$

The nonlinear equation was solved using the "fsolve" routine in MATLAB to obtain **G** and **F**. This was also used subsequently in the remaining numerical simulations. The numerical results for the control gains are:

$$\mathbf{G} = \begin{bmatrix} 7.6572 & 0 \\ 0 & 5.464 \end{bmatrix} 10^5 \ \mathrm{N/m} \ , \ \mathbf{F} = \begin{bmatrix} -69.3312 & 0 \\ 0 & 570.15 \end{bmatrix} \mathrm{Ns/m}$$

The result was validated using a state-space representation namely:

$$\mathbf{A} = \begin{bmatrix} \mathbf{0} & \mathbf{I} \\ \text{-}\mathbf{M}^{-1}(\mathbf{K}_b + \mathbf{K}_m + \mathbf{BGD}) & \text{-}\mathbf{M}^{-1}(\mathbf{C}_b + \mathbf{BFD}) \end{bmatrix} \tag{17}$$

which yields two pairs of poles: $-15 \pm 800i$ and $-49.99 \pm 3000i$. The closed-loop poles obtained are the same with the ones assigned. There is another stable pole added which is at $-6.9 \pm 7147.7i$. The open and closed loop displacement are plotted in Figure 4 represented by red and blue lines respectively. The location of the open and closed loop poles are shown in Figure 5 while the control force in both directions are shown in Figure 6.

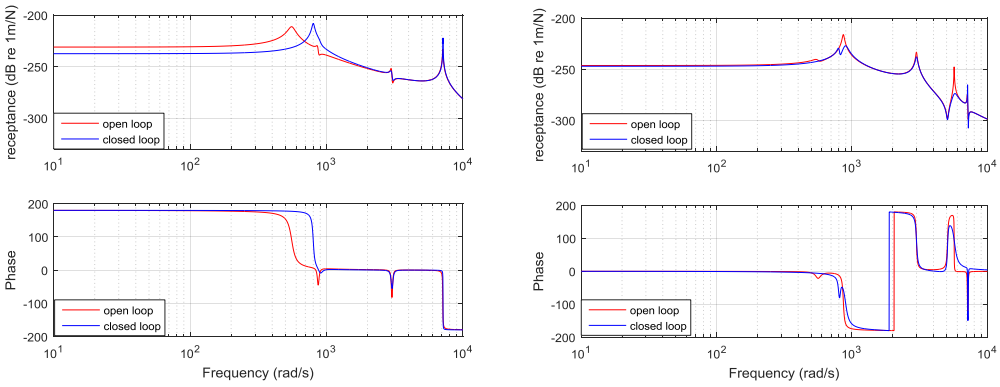

(a) (b)

Figure 4. Displacement per mesh excitation of the carrier in the horizontal and vertical directions with and without control due to mesh excitation.

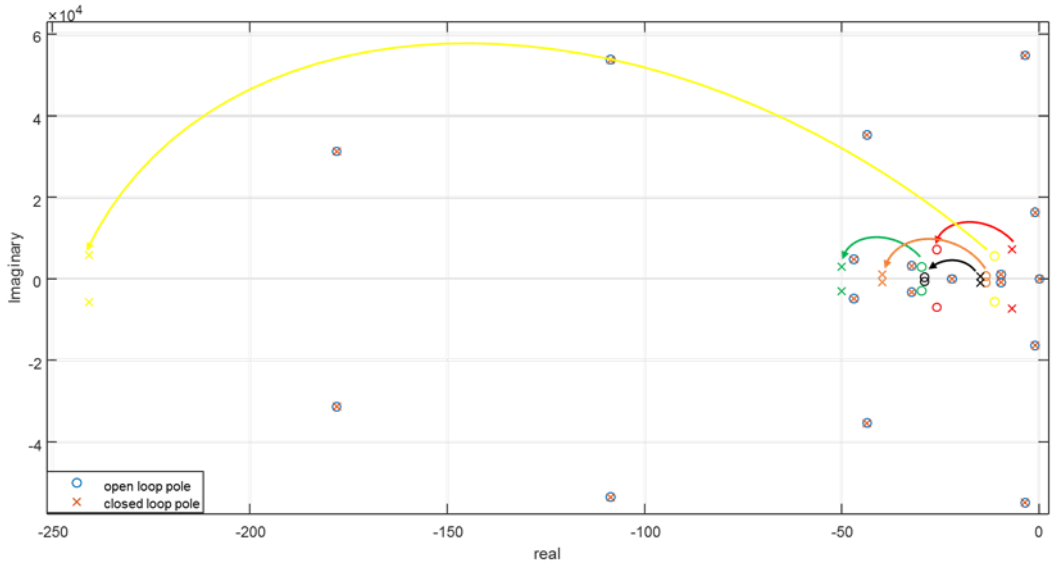

Figure 5. The *s*-plane plots showing the locations of the initial and the modified poles.

Figure. 4a shows that the level of damping was reduced at 800 rad/s, because the pole was shifted from $-29.33 \pm 555.42i$ to $-15 \pm 800i$. The damping level increases at 3000 rad/s because the open-loop pole was shifted from $-29.67 \pm 2993.21i$ to $-50 \pm 3000i$. The damping level at 7147.7 rad/s decreased because the closed loop pole was shifted from $-25.83 \pm 7119.35i$ to $-6.9 \pm 7147.7i$ but the natural frequency was shifted. Therefore, the closed loop poles assigned led to effective control on the four modes excited on the carrier in the horizontal direction.

In the vertical direction (Figure 4b), the closed-loop pole $-15 \pm 800i$ was added. A pole shifted from $-13.51 \pm 863i$ to $-39.83 \pm 893.87i$, which shows the reason why the damping in this direction increased. Damping was also added when the closed loop-pole was shifted from $-29.67 \pm 2993.21i$ to $-50 \pm 3000i$. The open-loop pole of the third excited pole shifted from $-11.267 \pm 5686i$ to $-24.089 \pm 5715.6i$ with significant damping added. In the fourth excited mode, the open-loop pole shifted from $-25.83 \pm 7119.25i$ to $-6.9 \pm 7147.7i$. This shows a reduction in the damping but a shift in the natural frequency. The closed-loop poles assigned also led to effective control in four translational modes excited in the vertical direction of the carrier.

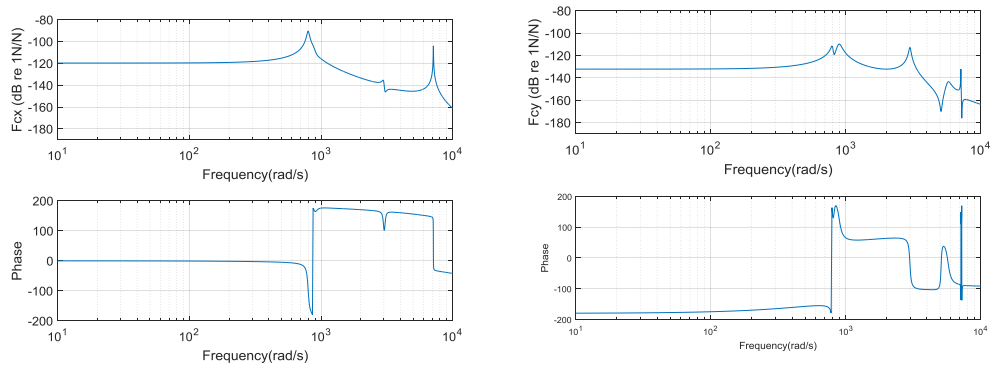

(a) (b)

Figure 6. Normalised control forces applied to the carrier in both the horizontal and vertical directions using a fixed frame of reference.

Figure 5 shows the five pairs of conjugate closed loop poles which were shifted in different colours. The arrows with different colours show their positions before and after they were shifted in s-plane.

They are all poles of translational modes where the carrier, ring and sun gears are translating in both the horizontal and vertical directions. This is because the poles were assigned to the carrier in the translational horizontal and vertical directions; therefore the poles shifted are those of translational modes only. The real and imaginary parts of the poles of the rotational modes remain unchanged.

The control forces, shown in Figure 6, depends on the control gains **G** and **F**, the closed-loop poles assigned and the amplitude of the excitation**.** Equation (2) shows the expression for the control force with the actuator distribution matrix **B**. The control forces in the horizontal direction is higher because the gain **G** corresponding to the stiffness is greater in the horizontal direction than the vertical direction. Generally, the control forces in both directions are relatively low compared to the excitation force.

4.2. Pole assignment to the carrier using a rotating frame of reference

The closed-loop pole was determined using the state space at the carrier speed of 100 rpm. In this case, $\bar{\mathbf{B}} = \mathbf{B}$, $\mathbf{D} = \bar{\mathbf{D}}$, $\bar{\mathbf{F}} = \mathbf{F}$.

It is assumed that the control gains in both frames of reference are not changing with time. Therefore, the control gains obtained using fixed frame of reference were assigned using the state space Equation (18) to obtain the poles.

$$\bar{\mathbf{A}} = \begin{bmatrix} \mathbf{0} & \mathbf{I} \\ -\bar{\mathbf{M}}^{-1}(\bar{\mathbf{K}}_b + \bar{\mathbf{K}}_m + \Omega_c \bar{\mathbf{K}}_d - \Omega_c^2 \bar{\mathbf{K}}_\Omega + \bar{\mathbf{B}}(\bar{\mathbf{G}} + \Omega_C \bar{\mathbf{F}}\mathbf{J})\bar{\mathbf{D}} & -\bar{\mathbf{M}}^{-1}(\bar{\mathbf{C}}_b + \bar{\mathbf{B}}\bar{\mathbf{F}}\bar{\mathbf{D}} + \Omega_C \mathbf{G}_y) \end{bmatrix} \tag{18}$$

Poles obtained at the carrier speed of 100 rpm are $-15.12 \pm 799.6i$ and $-49.96 \pm 2999.6i$.

These poles were assigned to the system in the horizontal and vertical directions of the carrier. This yields the following control gains

$$\bar{\mathbf{G}} = \begin{bmatrix} 7.6566 & 0 \\ 0 & 5.4530 \end{bmatrix} 10^5 \text{ N/m}, \quad \bar{\mathbf{F}} = \begin{bmatrix} -69.3312 & 0 \\ 0 & 570.10 \end{bmatrix} \text{Ns/m}$$

The results was validated by the state-space method, Equation (18), and it yields the following poles

$$-15.11 \pm 799.58i \text{ and } -49.96 \pm 2999.6i \quad .$$

The poles are the same as the closed loop poles assigned.

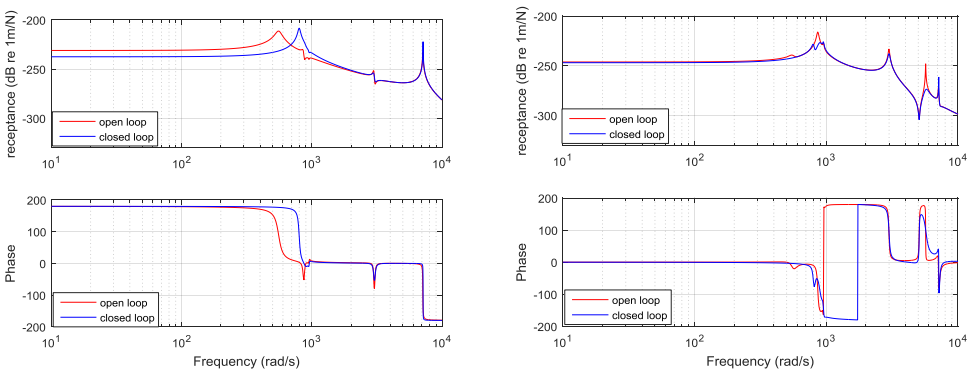

(a) (b)

Figure 7. Displacement per mesh excitation of the carrier in the horizontal and vertical directions with and without control due to mesh excitation at the carrier speed 100 rpm.

The natural frequency was shifted from 555.41 to 800 rad/s, but the level of damping in the horizontal direction of the carrier has reduced (Figure(7(a)). There is a frequency of a higher mode (7119.25 rad/s) which was shifted to 7147.7 rad/s. The behaviour of the carrier in both the horizontal and vertical directions at 100 rpm is the same as its behaviour using the fixed frame of reference. In summary, the behaviour of the carrier using either a fixed or rotating frame of reference are the same provided the carrier speed is relatively low.

The shift in the poles are the same as they are moving using the fixed frame of reference. The control force in the horizontal direction is higher than that necessary in the vertical directions. The same magnitude of control forces are needed using either frame of reference for analysis.

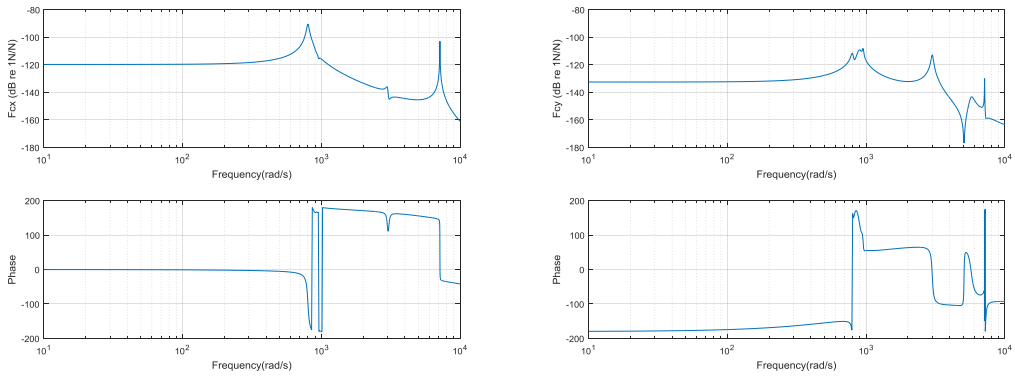

(a) (b)

Figure 8. Normalised control forces on the carrier in both the horizontal and vertical directions using a rotating frame of reference at the carrier speed 100 rpm.

5. Numerical example of pole assignment to the sun gear

The method of pole placement will now be applied to the sun gear in the vertical and horizontal directions simultaneously using both frames of reference. The pole placement on the sun gear will be compared to that of the carrier, in order to determine the best location to apply the actuator to the system.

5.1. Pole assignment to the sun gear using a fixed frame of reference

Two conjugate poles (which are the same assigned to the carrier) were assigned to the sun gear assuming two actuators acting at the sun gear in the horizontal and vertical directions. The corresponding actuator distribution matrix $\mathbf{B} \in \Re^{15\times 2}$ and the sensor distribution matrix $\mathbf{D} \in \Re^{2\times 15}$ were chosen to be

$$\mathbf{D} = \mathbf{B}^{\mathrm{T}} = \begin{bmatrix} 0 & 0 & 0 & 0 & 0 & 0 & 1 & 0 & 0 & 0 & 0 & 0 & 0 & 0 & 0 \\ 0 & 0 & 0 & 0 & 0 & 0 & 0 & 1 & 0 & 0 & 0 & 0 & 0 & 0 & 0 \end{bmatrix}$$

In this case $q_{1op} = x_s$ and $q_{2op} = y_s$.

The open-loop displacement per mesh excitation are at the values of s corresponding to the chosen closed loop poles

$$\mathbf{H}(\lambda_j) = (\mathbf{M}\lambda_j^2 + \mathbf{C}_b\lambda_j + \mathbf{K}_b + \mathbf{K}_m)^{-1}, \quad j = 1,....,4$$

The four characteristic equations can be written as

$$\det(\mathbf{I} + \mathbf{H}(\lambda_j)\mathbf{B}(\mathbf{G} + \lambda_j\mathbf{F})\mathbf{B}^{\mathrm{T}}) = 0, \quad j = 1,....,4$$

which are nonlinear equations for evaluation of the control gains **G** and **F**. The subsequent result for the control gains are:

$$\mathbf{G} = \begin{bmatrix} 1.7314\times 10^7 & 0 \\ 0 & -3.4090\times 10^5 \end{bmatrix} \mathrm{N/m}, \mathbf{F} = \begin{bmatrix} 944.24 & 0 \\ 0 & 10.4567 \end{bmatrix} \mathrm{Ns/m}$$

The result was validated by the state-space method. This yields $-15 \pm 800i$ and $-49.99 \pm 3000i$ as the poles. The closed-loop poles obtained are the same as the ones assigned.

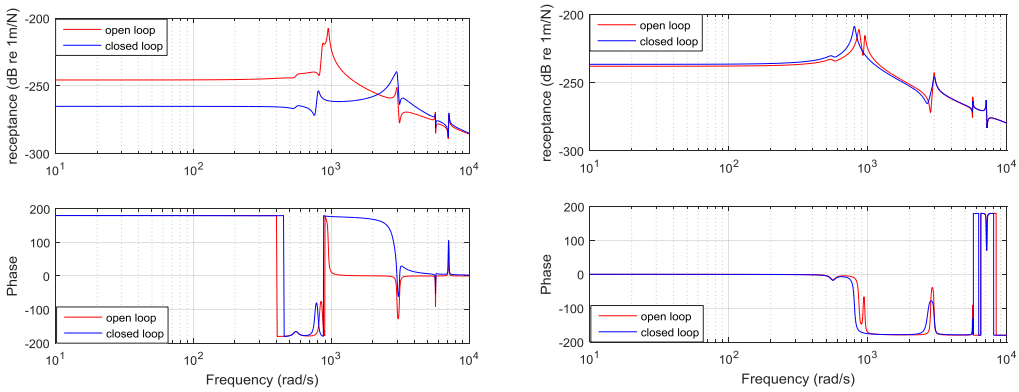

(a) (b)

Figure 9. Displacement per mesh excitation of the sun gear in the horizontal and vertical directions with and without control due to mesh excitation.

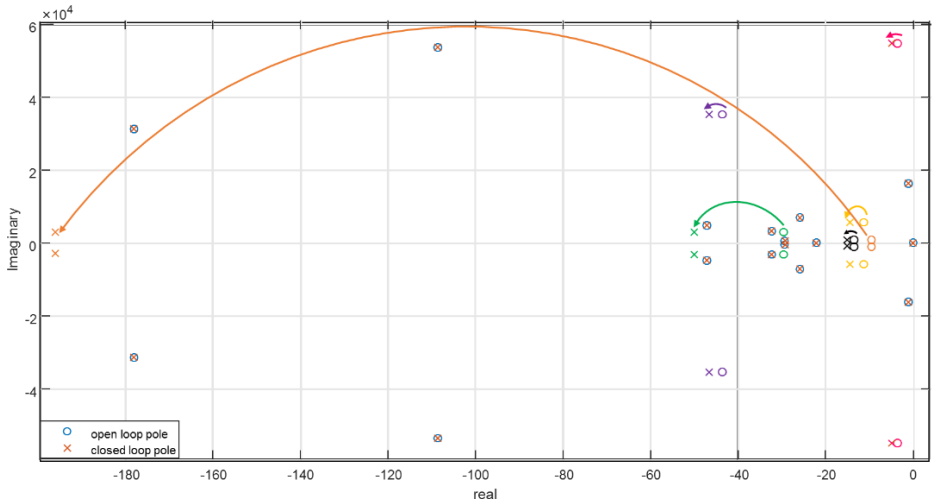

Figure 10. The *s*-plane showing the initial and modified poles when two actuators were applied on the sun gear.

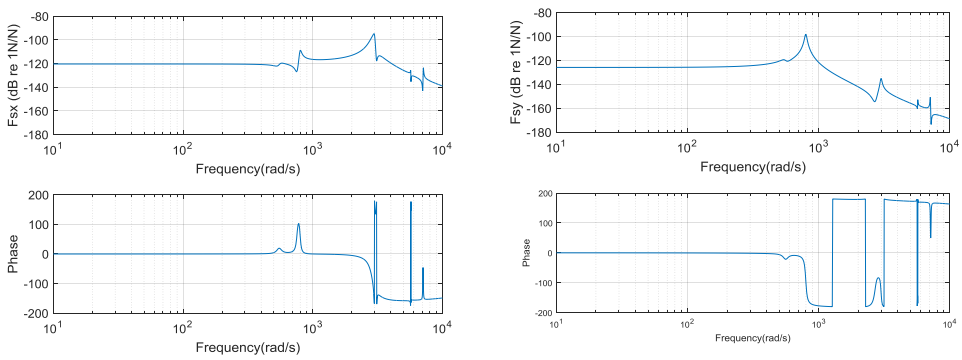

(a) (b)

Figure 11. Normalised control forces on the sun gear in both the horizontal and vertical directions.

5.2. Pole assignment to the sun gear using a rotating frame of reference

The assigned poles were obtained using the control gains determined from fixed frame of reference in the state space equation of rotating frame of reference at the carrier speed of 100 rpm. The closed-loop

pole are $\lambda_{1,2} = -15 \pm 800i$ and $\lambda_{2,3} = -49.99 \pm 2999.6i$. These poles were assigned and the following control gains **G** and **F** were obtained:

$$\bar{\mathbf{G}} = \begin{bmatrix} 1.7310\times10^{7} & 0 \\ 0 & -3.4275\times10^{5} \end{bmatrix} \mathrm{N/m}, \quad \bar{\mathbf{F}} = \begin{bmatrix} 943.77 & 0 \\ 0 & 11.0948 \end{bmatrix} \mathrm{Ns/m}$$

The results was validated by the state-space method yielding pole at $-15.13 \pm 799.60i$ and $-49.99 \pm 2999.6i$. The closed-loop poles obtained are almost the same as the ones assigned. The shift in the poles are also the same as they are moving using the fixed frame of reference.

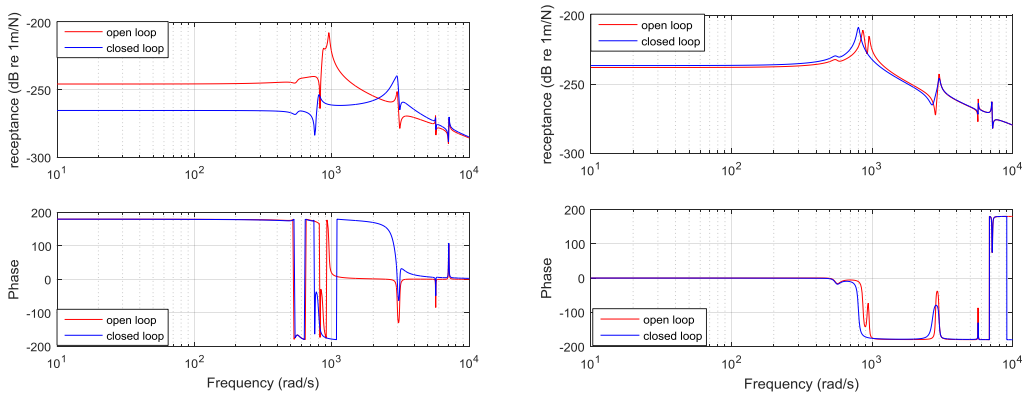

(a) (b)

Figure 12. Displacement per mesh excitation of the sun gear in the horizontal and vertical directions with and without control due to mesh excitation using a rotating frame of reference.

Two actuators were used to assign two pairs of conjugate poles to the sun gear in both the horizontal and vertical directions using the fixed frame of reference. The responses are shown in Figure 9(a) and (b). The peak of the first excited mode in the horizontal direction disappeared completely (Figure. 9(a)). It is obvious that a significant level of damping was added. This is because the control gain in the **F** matrix, corresponding to active damping in the horizontal direction, is very high. A closed loop pole whose damped natural frequency is 800 rad/s can be seen. The frequency of the second excited mode shifted from 2993 to 3000 rad/s. There is no significant change at high frequencies 5686 and 7119 rad/s. In the vertical direction (Figure 9(b)), the frequency of the first mode shifted from 862.8 to 800 rad/s because of the negative value of active stiffness in the **G** matrix. The second peak disappears after the pole assignment, while the peak at 2993 rad/s shifted to 3000 rad/s with little damping added. The sun gear exhibits the same behaviour using rotating frame of reference (Figure 12(a) and (b)).

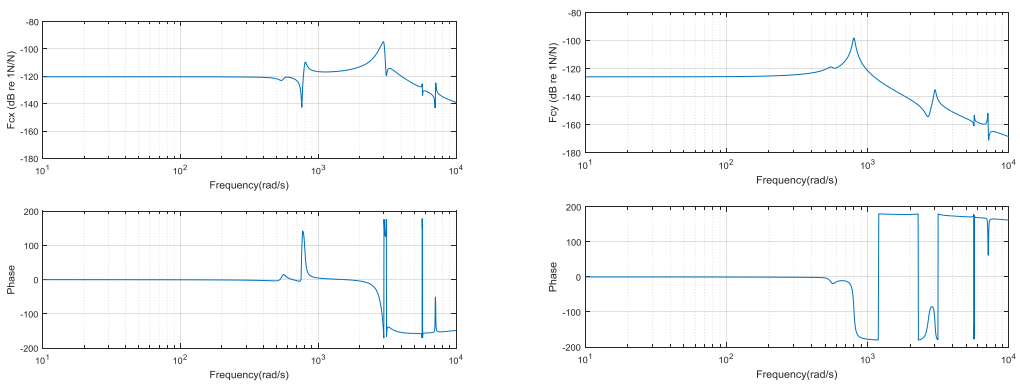

(a) (b)

Figure 13. Normalised control forces on the sun gear in both the horizontal and vertical directions using a rotating frame of reference.

6. Conclusions

Planetary gear vibration control by pole placement method using output feedback has been presented and numerically implemented. The same poles were assigned to the carrier and sun gear in the horizontal and vertical directions using both the fixed and rotating frames of reference. It is shown that for active stiffness, pole placement on the carrier shows better vibration control than application to the sun gear. For active damping, the pole placement on the sun gear shows better vibration control. The simultaneous assignment of a pole to both the carrier and sun gear will show a better vibration control than assigning the poles to one of them. The frequencies of the translational modes were shifted and damped, while the frequencies of the rotational modes remain unchanged. In addition, it has been shown that the control force determined using a rotating frame of reference can be transformed to the fixed frame of reference for practical implementation.

References

[1] Cooley C G. and R G Parker 2014, *A review of planetary and epicyclic gear dynamics and vibrations research.* Applied Mechanics Reviews, **66**(4): p. 040804.
[2] McFadden P and J Smith 1985, *An explanation for the asymmetry of the modulation sidebands about the tooth meshing frequency in epicyclic gear vibration.* Proceedings of the Institution of Mechanical Engineers, Part C: Journal of Mechanical Engineering Science, **199**(1): p. 65-70.
[3] Seager D L 1975, *Conditions for the Neutralization of Excitation by the Teeth in Epicyclic Gearing.* Mechanical Engineering Science, I Mech E, **5**: p. 293 - 299.
[4] Parker R G 2000 *A physical explanation for the effectiveness of planet phasing to suppress planetary gear vibration.* Journal of Sound and Vibration, **236**(4): p. 561-573.
[5] Richards D and D J Pines 2003, *Passive reduction of gear mesh vibration using a periodic drive shaft.* Journal of Sound and Vibration, **264**(2): p. 317-342.
[6] Tharmakulasingam R., G Alfano and M Atherton 2008,. *Reduction of gear pair transmission error with tooth profile modification* (Middlesex: Brunnel University).
[7] Montague G T, Ksack A F, Palazzolo A, Manchala D and Thomas E, 1994, *Feedforward control of gear mesh vibration using piezoelectric actuators.* Shock and Vibration,. **1**(5): p. 473-484.
[8] Rebbechi B, Howard C and Hansen C 1999 *Active control of gearbox vibration*. in *INTER-NOISE and NOISE-CON Congress and Conference Proceedings*.. Institute of Noise Control Engineering.
[9] Mottershead J E, Tehrani M G, James S and Ram Y M, 2008 *Active vibration suppression by pole-zero placement using measured receptances.* Journal of Sound and Vibration, **311**(3): p. 1391-1408.
[10] Parker R.G 1999., *Analytical Characterization of Unique Properties of Planetary Gear Free Vibration.* Transactions of ASME **121**(July 1999): p. 316 - 321.